

Online Learning Koopman operator for closed-loop electrical neurostimulation in epilepsy

Zhichao Liang[†], Zixiang Luo[†], Keyin Liu, Jingwei Qiu and Quanying Liu^{*}

Abstract—Electrical neuromodulation as a palliative treatment has been increasingly used in epilepsy. However, most current neuromodulations implement pre-determined actuation strategies and lack self-adaptive patterns for adjusting stimulation strategies. In this work, rooted in optimal control theory, we propose a novel framework for real-time closed-loop electrical neuromodulation in epilepsy, which combines i) a deep Koopman operator based dynamical model to predict the temporal evolution of epileptic EEG with an approximated finite-dimensional linear dynamics and ii) a model predictive control (MPC) modular to design optimal seizure suppression strategies. It is termed *Koopman-MPC framework*. The Koopman operator based linear dynamical model is embedded in the latent state space of the autoencoder neural network, in which we can approximate and update the Koopman operator online. The linear dynamical property of the Koopman operator ensures the convexity of the optimization problem for subsequent MPC control. The predictive capability of the deep Koopman operator model is tested with both synthetic and real epileptic EEG data. The results demonstrate that the deep Koopman operator based model can map nonlinear neural dynamics into finite-dimensional linear dynamics with higher performance in predicting the seizure dynamics, compared with a 10-order autoregressive model (AR) model and a recurrent neural network (RNN). Moreover, compared with the RNN-MPC framework, the Koopman-MPC framework can better suppress seizure dynamics with less time consumption (only 0.035s), enabling real-time updates of epilepsy control strategies. Our Koopman-MPC framework opens a new window for model-based closed-loop neuromodulation and sheds light on nonlinear neurodynamics and feedback control policies.

Index Terms—Electrical Neuromodulation, Closed-loop Neuromodulation, Deep Koopman operator, Model Predictive Control, Online Learning.

EPILEPSY is a neurological disorder characterized by the occurrence of spontaneous epileptic seizures, during which the neuronal population fire in an abnormal, excessive, and synchronized manner [1], [2]. Clinically, the main biomarkers for the diagnosis of epilepsy are epileptiform spikes, seizure-like waves and high-frequency oscillations, which are usually monitored by electroencephalogram (EEG), stereoelectroencephalogram (sEEG), and intracranial electroencephalogram (iEEG) [3], [4], [5].

This work was funded in part by the National Key Research and Development Program of China (2021YFF1200800), National Natural Science Foundation of China (62001205), Shenzhen-Hong Kong-Macao Science and Technology Innovation Project (SGDX2020110309280100), Guangdong Natural Science Foundation Joint Fund (2019A1515111038), Shenzhen Science and Technology Innovation Committee (20200925155957004, KCXFZ2020122117340001), Shenzhen Key Laboratory of Smart Healthcare Engineering (ZDSYS20200811144003009).

Z. Liang, Z. Luo, K. Liu, J. Qiu and Q. Liu are with Shenzhen Key Laboratory of Smart Healthcare Engineering, Department of Biomedical Engineering, Southern University of Science and Technology, Shenzhen, 518055, P. R. China.

[†] Co-first authors: Zhichao Liang, Zixiang Luo

^{*} Corresponding author: Quanying Liu liuqy@sustech.edu.cn

A range of treatments have been developed to control seizures, including anti-epilepsy medication, palliative/radical surgery, and electrical neurostimulation [2], [6], [7], [8], [9]. Compared with surgery, electrical neurostimulation, such as deep brain stimulation (DBS) and transcranial electrical stimulation (TES), has fewer long-term side effects on brain function, and has been becoming a considerable clinical intervention for intractable epilepsy [8], [10], [11]. Electrical neurostimulation applies a minuscule dose of high-frequency electric current (e.g., 50 Hz) to a specific targeting region [12], such as the mesial temporal cortex (0.5 mA ~ 5 mA), or neocortex (0.5 mA ~ 8 mA), aiming at modulating neural oscillations and thereby driving the seizure state to a seizure-free state [13], [8], [12].

However, current neuromodulation mainly implements pre-determined open-loop actuation strategies, rather than a closed-loop real-time updated stimulation strategy. The open-loop neurostimulation actually lacks feedback signals from the observed real-time seizure waves for adjusting the control inputs during neurostimulation, which would limit its flexibility in practical applications [9]. More recently, closed-loop neuromodulation is increasingly gaining attention in clinical applications such as seizure control [8], [9], [14], [15] and Parkinson disease treatment [16], [17]. By framing the neuromodulation to a closed-loop state-space control problem, the main goal then is to design an optimal control law to steer the present system state to the desired state. Some pioneer works have been devoted to this area, ranging from designing state-space models to control methods. For example, Sérgio Pequito et al. presented a spectral control method to ensure that the poles of a closed-loop system are within the pre-specified spectrum range [18]. Arian Ashourvan et al. proposed a linear time-invariant switching system for modelling seizure dynamics, combined with a pole-placement spectral static output feedback control-theoretic strategy for suppressing seizure dynamics [19]. Recently, model predictive control (MPC), as a self-tuning control method to maintain a stable and robust control process, has also been brought into neurostimulation applications [20], [21]. For instance, Siyuan Chang et al. presented a nonlinear auto-regressive moving-average (NARMA) Volterra model to identify the input-output relationship between external inputs and corresponding neuronal responses (such as synthetic seizure-like waves), based on which a closed-loop MPC-driven actuation strategy was implemented to optimize the stimulator [20]. Sarthak Chatterjee et al. proposed a fractional-order model based MPC framework in neuromodulation [21]. In general, MPC is a model-based optimal control framework, which requires developing a predictive model to characterize system dynamics with high accuracy and to facilitate the solution

of optimization problem with low computational complexity. However, the trade-off between accuracy and complexity is particularly challenging for developing a model to balance the two in the MPC framework.

Seizure dynamics is a complex networked nonlinear dynamic process, which we have not yet fully understood [22], [23], [24]. A seizure control task calls for modeling the underlying complex seizure dynamics and obtaining its control law for seizure suppression, as opposed to the seizure detection or classification tasks with end-to-end deep learning solutions [25], [26], [27], [28]. Therefore, system identification is crucial for uncovering the system dynamics over the seizure period by building mathematical models for the underlying system and estimating model parameters based on the observed input-output data. Several traditional system identification methods have been used to model the seizure system dynamics with EEG data, such as the auto-regressive moving-average model [20] and the fractional-order system model [21]. With advances in machine learning, data-driven models based on neural networks show great potential as system identification tools [29], [30], [31], [32], [33]. For instance, recurrent neural networks (RNNs) have proven promising in fitting time-series data and modeling dynamical systems in fluidic flow control [33] and process industries [31]. However, RNN models are quite complex and highly nonlinear when integrated into a MPC framework for real-time optimization control, which will become a non-convex optimization problem that is computationally inefficient.

When modeling seizure dynamics and designing seizure suppression controllers, it is necessary to consider the trade-off between model accuracy and complexity. The former allows to approximate nonlinear seizure system with high prediction performance, while the latter guarantees computational efficiency for solving MPC optimizations. The optimal solution to a non-convex optimization problem, originated from the MPC of nonlinear complex dynamical model, is numerical computational inefficiency and challenging to obtain the optimal solution. Operator-theoretic approaches, mainly based on the Perron-Frobenius operator [34] or its adjoint Koopman operator, can approximate a nonlinear dynamical system with linear operators, bringing a new direction to solve this problem. In particular, Koopman theory (Fig. 1) states that a nonlinear dynamical system can be linearized under the assumption that the linear operator acts on the observation function of system states over time [35]. However, the pre-defined Koopman operator model has substantial limitations in modeling time-varying or complex switching dynamical systems. Therefore, a more flexible way to approximate the finite-dimensional Koopman operator in an invariant subspace is needed [36]. Recently, autoencoder architecture has been employed to learn the finite-dimensional Koopman operator without the necessity of a hand-crafted design of Koopman operator [37], [36]. Lying on the linear properties and online learning Koopman operator in invariant subspace, the Koopman-based MPC framework has strong capabilities for the closed-loop neurostimulation in both model accuracy and complexity.

In this study, we propose a deep Koopman operator based

model predictive control framework (*i.e.*, Koopman-MPC framework) for closed-loop seizure suppression in a real-time manner. The Koopman-MPC framework can meet the needs of sufficient prediction accuracy and low model complexity for real-time optimization. The contributions of this study are summarized as follows.

- A Koopman-MPC framework is proposed (**Sec. I**), including a *Koopman operator based linear dynamical model* embedded into a finite-dimensional invariant subspace, and a *MPC controller* to optimize the neurostimulation policy for seizure control. The design of Koopman-based model leverages the flexibility of online learning of Koopman operator, and enables real-time optimization for MPC controller.
- A deep autoencoder neural network is employed to learn, rather than to hand-crafted design, the embedding linear invariant subspace (**Sec. II**). Experimental results demonstrate that the deep Koopman operator model outperforms the AR model and RNN model in seizure prediction, for both synthetic data and real epileptic data (**Sec. III-C**). The spectral analysis of the estimated Koopman operator provides a biomarker of seizure onset (Fig. 8(C) & Fig.9).
- The seizure suppression performance of the Koopman-MPC framework is validated and compared with the baseline RNN-MPC framework, using a virtual platform based on the Jansen-Rit model. The results show that Koopman-MPC framework successfully suppresses seizure dynamics with higher computational efficiency (**Sec. III-D**) and allows online learning of the Koopman operator for closed-loop epilepsy control (**Sec. III-E**).

I. METHOD

In this section, we first introduce the Koopman operator theory and its extension to the linear forced dynamical systems, then we propose the Koopman operator based model predictive control for online optimization of the optimal control signals over the Koopman observations.

A. Koopman operator

Consider a nonlinear discrete-time dynamical system that satisfies

$$\mathbf{x}_{i+1} = f(\mathbf{x}_i), \quad (1)$$

where $\mathbf{x}_i \in \mathcal{M} \subset \mathbb{R}^n$ denotes the vector of state variables at time step i and the function $f(\cdot) : \mathcal{M} \rightarrow \mathcal{M}$ governs nonlinear dynamics of the system under a finite low-dimensional manifold \mathcal{M} , in which the future state \mathbf{x}_{i+1} only depends on the current state \mathbf{x}_i .

According to the Koopman operator theory, there exists an infinite-dimensional linear operator \mathbf{K} acting on an infinite-dimensional function space such that the observation functions $g(\cdot)$ satisfy an advancing forward linear relation, as shown in Fig. 1.

$$g(\mathbf{x}_{i+1}) = \mathbf{K}g(\mathbf{x}_i) = g \circ f(\mathbf{x}_i). \quad (2)$$

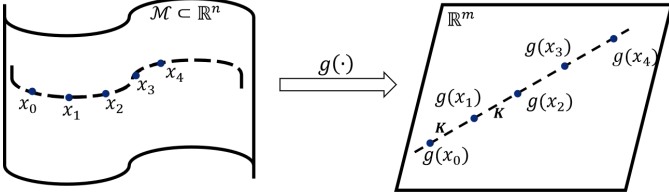


Fig. 1. Koopman operator theory. $g(\cdot)$ is a transformation from a nonlinear manifold space $\mathcal{M} \subset \mathbb{R}^n$ to a linear manifold space \mathbb{R}^m , where a linear forward relation K can be inferred.

The modal decomposition of Koopman operator \mathbf{K} refers to spectral analysis [38], in which its modes and eigenvalue-eigenvector pairs characterize the complex dynamical behaviours as a linear combination of independent spatiotemporal patterns.

$$\mathbf{K} = V D V^T \quad (3)$$

where $D = \text{diag}\{d_1, d_2, \dots\}$ is the eigenvalue matrix and $V = [V_1, V_2, \dots]$ is the eigenvector matrix.

Specifically, the eigenvalue d_i of \mathbf{K} is a complex value which reflects system stability, exponential damping ratio and spectral information, and eigenvector V_i represents the independent spatial coordinates. Based on the linear Koopman operator \mathbf{K} and the current state \mathbf{x}_i , the future evolution of states are feasibly predictable, thereby compatible with the subsequent MPC control of system dynamics.

One nonnegligible issue about the Koopman operator modeling is how to design (or to learn) the nonlinear embedding function $g(\cdot)$ in infinite-dimensional space which allows transforming a nonlinear dynamical system into a linear dynamical system. A variety of methods have been proposed to design the finite-dimensional embedding function $\hat{g}(\cdot)$ to approximate the infinite-dimensional space (*i.e.* the extended dynamic mode decomposition [39], [40] and auto-encoder [37], [36]).

As a data-driven method, the extended dynamic mode decomposition allows arbitrary composition of a set of basis functions (*e.g.*, $\Phi_1, \Phi_2, \dots, \Phi_m$) of nonlinear dynamics, which has been commonly used for the numerical approximation of the Koopman operator $\hat{\mathbf{K}}$ [39].

Given a finite sequence of system state measurements \mathbf{x}_i ($i = \{0, 1, \dots, n\}$), and a finite set of basis functions (*e.g.*, $\Phi_1, \Phi_2, \dots, \Phi_m$), we constitute a basis function vector $\Phi = [\Phi_1, \Phi_2, \dots, \Phi_m]^T$, and then embed the data series \mathbf{x}_i into the basis function vector to construct two feature states Ψ_X and $\Psi_{\hat{X}}$, as follows:

$$\begin{aligned} \Psi_X &= [\Phi(\mathbf{x}_0) \ \Phi(\mathbf{x}_1) \ \dots \ \Phi(\mathbf{x}_{n-1})] \in \mathbb{R}^{m \times n} \\ \Psi_{\hat{X}} &= [\Phi(\mathbf{x}_1) \ \Phi(\mathbf{x}_2) \ \dots \ \Phi(\mathbf{x}_n)] \in \mathbb{R}^{m \times n} \end{aligned} \quad (4)$$

According to the least-square estimation, the finite-dimensional approximation of the Koopman operator $\hat{\mathbf{K}} \in \mathbb{R}^{m \times m}$ can be inferred as

$$\hat{\mathbf{K}} = \Psi_{\hat{X}} \Psi_X^\dagger \quad (5)$$

where Ψ_X^\dagger is defined as $\Psi_X^\dagger = \Psi_X^T (\Psi_X \Psi_X^T + \lambda \mathbf{I})^{-1}$, and λ is the regularization factor.

The approximated linear dynamical system can be rewritten as

$$\Phi(\mathbf{x}_{i+1}) = \hat{\mathbf{K}} \Phi(\mathbf{x}_i). \quad (6)$$

Also, we consider a forced nonlinear dynamics with input \mathbf{u}_i ,

$$\mathbf{x}_{i+1} = f(\mathbf{x}_i, \mathbf{u}_i), \quad (7)$$

where $\mathbf{u}_i \in \mathbb{R}^{r \times 1}$ is a r -dimension control input at time step i , namely there are r inputs in this system.

Then, we extend the approximated Koopman operator based linear dynamical system into a linear forced control dynamical system, in which we only substitute the Eq. (6) into Eq. (8). In this case, the objective is simultaneously to learn an approximated finite-dimensional representation space of the state variables and its relationship with control inputs.

$$\begin{aligned} \Phi(\mathbf{x}_{i+1}) &= \hat{\mathbf{K}} \Phi(\mathbf{x}_i) + \hat{\mathbf{B}} \mathbf{u}_i \\ &= [\hat{\mathbf{K}}, \hat{\mathbf{B}}] \begin{bmatrix} \Phi(\mathbf{x}_i) \\ \mathbf{u}_i \end{bmatrix}. \end{aligned} \quad (8)$$

where $\hat{\mathbf{B}} \in \mathbb{R}^{m \times r}$ is the control matrix. Then, the approximated Koopman operator and the control matrix can be inferred from

$$[\hat{\mathbf{K}}, \hat{\mathbf{B}}] = \Psi_{\hat{X}} \hat{\Psi}_X^\dagger, \quad (9)$$

where $\hat{\Psi}_X = \begin{bmatrix} \Psi_X \\ U \end{bmatrix} = \begin{bmatrix} \Phi(\mathbf{x}_1) & \Phi(\mathbf{x}_2) & \dots & \Phi(\mathbf{x}_n) \\ \mathbf{u}_1 & \mathbf{u}_2 & \dots & \mathbf{u}_n \end{bmatrix}$ is the augmented state.

In this study, we design a deep autoencoder neural network as the basis function to learn the finite-dimensional linear invariant subspace in a self-supervised manner (Sec. II) instead of the hand-crafted basis function $\Phi(\cdot)$.

B. Koopman-MPC framework

Model predictive control is an optimization-based control framework. It minimizes the objective function in a finite prediction horizon with the control inputs and states transition constraints. The MPC optimization for highly nonlinear dynamical systems is a nonconvex problem of NP-hardness, and we prefer to treat it as the MPC convex optimization problem for linear systems with an unique solution.

The predictive capability and linearity of the approximated Koopman operator facilitates the model predictive controller design for nonlinear systems. We transform the nonlinear dynamical system MPC problem into an approximated Koopman operator based linear MPC problem.

In this study, we construct a Koopman operator based model predictive control framework to control the nonlinear seizure dynamical system following the desired reference signals (seizure-free signals), as shown in Fig. 2. At each time step, the model predictive controller solves the following objective function by quadratic programming solver to find a sequence

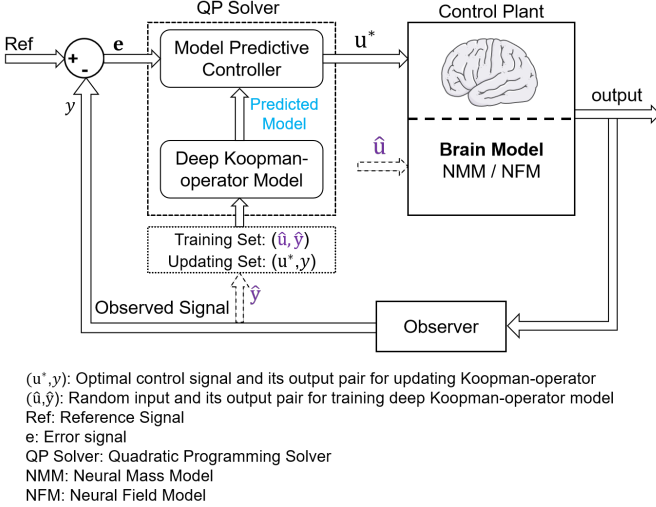


Fig. 2. The Koopman operator based MPC closed-loop neurostimulation framework. The control plant can be the brain system or other computational brain model (Neural Mass Model or Neural Field Model). In the training period (the dotted arrow), the system is identified by the collected input-output pair (\hat{u}, \hat{y}) . During the control period, the approximated Koopman operator and control matrix can be updated by collecting input-output pairs (u^*, y) . We term it online learning. The Koopman operator based model predictive controller is optimized by quadratic programming solver.

of incremental inputs $\Delta \mathbf{u}_i$ ($i = 1, 2, \dots, T_c$) and only the first incremental input $\Delta \mathbf{u}_1$ will be applied to the system.

$$\begin{aligned} \min_{\Delta \mathbf{u}} \quad & \sum_{i=1}^{T_p} (\Phi(\mathbf{x}_i) - \Phi(\mathbf{x}_{ref}))^T \mathbf{Q}_X (\Phi(\mathbf{x}_i) - \Phi(\mathbf{x}_{ref})) \\ & + \sum_{i=1}^{T_c} \Delta \mathbf{u}_i^T \mathbf{Q}_u \mathbf{u}_i \\ \text{s.t.} \quad & \Delta \mathbf{u}_i \in [\Delta \mathbf{u}_{\min}, \Delta \mathbf{u}_{\max}] \\ & \mathbf{u}_i = \mathbf{u}_{i-1} + \Delta \mathbf{u}_i \\ & \mathbf{u}_i \in [\mathbf{u}_{\min}, \mathbf{u}_{\max}] \\ & \Phi(\mathbf{x}_{i+1}) = \hat{\mathbf{K}}\Phi(\mathbf{x}_i) + \hat{\mathbf{B}}\mathbf{u}_i \end{aligned} \quad (10)$$

where T_p and T_c are the length of predictive horizon and control horizon, respectively. $\Phi(\mathbf{x}_i)$ and $\Phi(\mathbf{x}_{ref}) \in \mathbb{R}^{m \times 1}$ are the finite dimensional representation of the system state \mathbf{x}_i and reference signals \mathbf{x}_{ref} in the Koopman invariant subspace, respectively. $\Delta \mathbf{u}_i \in \mathbb{R}^{r \times 1}$ (r is the number of system inputs) is the increment of input at step i . $\mathbf{Q}_X \in \mathbb{R}^{m \times m}$ is the positive definite weighted matrix for penalizing the deviance and $\mathbf{Q}_u \in \mathbb{R}^{r \times r}$ is a non-negative matrix for penalizing the amplitudes of control incremental inputs and tune the desired closed-loop control performance. For real applications, the inputs are constrained between the upper bound and lower bound. The equation $\Phi(\mathbf{x}_{i+1}) = \hat{\mathbf{K}}\Phi(\mathbf{x}_i) + \hat{\mathbf{B}}\mathbf{u}_i$ is the linear state transition constraint condition that predicts the future states in the predictive horizon. $\hat{\mathbf{K}}$ is either the approximated unforced Koopman operator when given no inputs or the forced Koopman operator when given inputs [37]. $\hat{\mathbf{B}} \in \mathbb{R}^{m \times r}$ can be inferred by Eq. (9). This optimization problem can be solved efficiently with the quadratic programming solver. In this study, the input signals are constrained from -30 to 5 and the increment of inputs signals are constrained from -20 to

0.5. \mathbf{Q}_X is set to be an identity matrix \mathbb{I} . \mathbf{Q}_u equals to $0.01\mathbb{I}$.

II. DEEP KOOPMAN OPERATOR BASED SEIZURE DYNAMICAL MODEL

We design an autoencoder framework with fully-connected layers to learn a finite dimensional invariant subspace, where we can approximate or update the Koopman operator in the proposed deep Koopman operator model shown in Fig.3.

A. Autoencoder Architecture to Predict Seizure Dynamics

The Koopman operator based autoencoder consists of an encoder and a decoder neural network, both of which contain three fully-connected layers. The first two layers are followed by a hyperbolic tangent activation function (tanh), while the last layer has no activation function and directly generates the output. The parameter settings of each layer of networks are described in the Appendix (Table IV).

As shown in Fig.3, X and Y are two segments of signal input to the model, where $X = [x_0, x_1, \dots, x_{n-1}] \in \mathbb{R}^{k \times n}$ denotes the past n steps of data and $Y = [x_1, x_2, \dots, x_n] \in \mathbb{R}^{k \times n}$ denotes the past $n-1$ steps of data and the current state $x_n \in \mathbb{R}^{k \times 1}$. k is the dimension of the original system state space. The encoder embeds the low-dimensional input data into a higher-dimensional latent space and generates $\hat{X}, \hat{Y} \in \mathbb{R}^{m \times n}$ ($m > k$),

$$\hat{X} = \text{encoder}(X), \quad \hat{Y} = \text{encoder}(Y) \quad (11)$$

The following two cases are considered in the linear dynamical system within the finite dimensional space.

(1) Without external inputs.

In this case, the prediction process is governed by

$$\hat{x}_{n+1} = \hat{\mathbf{K}}\hat{x}_n. \quad (12)$$

We estimate $\hat{\mathbf{K}}$ by solving the linear least squares problem of $\hat{Y} = \hat{\mathbf{K}}\hat{X}$. Where $\hat{\mathbf{K}} = \hat{Y}\hat{X}^\dagger$, and \hat{X}^\dagger is the pseudo inverse of \hat{X} .

(2) With external inputs.

In this case, we consider the basic linear forced dynamical system for prediction

$$\hat{x}_{n+1} = \hat{\mathbf{K}}\hat{x}_n + \hat{\mathbf{B}}u_n = [\hat{\mathbf{K}}, \hat{\mathbf{B}}] \begin{bmatrix} \hat{x}_n \\ u_n \end{bmatrix}. \quad (13)$$

We estimate the Koopman operator $\hat{\mathbf{K}}$ and control matrix $\hat{\mathbf{B}}$ with \hat{X}, \hat{Y} and input series $U = [u_0, u_1, \dots, u_{n-1}]$

$$[\hat{\mathbf{K}}, \hat{\mathbf{B}}] = \hat{Y} \begin{bmatrix} \hat{X} \\ U \end{bmatrix}^\dagger \quad (14)$$

where $\begin{bmatrix} \hat{X} \\ U \end{bmatrix}^\dagger$ is the augmented state of \hat{X} and U .

We transform \hat{X} and \hat{x}_{n+i} ($i = 1, 2, \dots, T_p$) back into the original state space

$$\tilde{X} = \text{decoder}(\hat{X}), \quad \tilde{x}_{n+i} = \text{decoder}(\hat{x}_{n+i}). \quad (15)$$

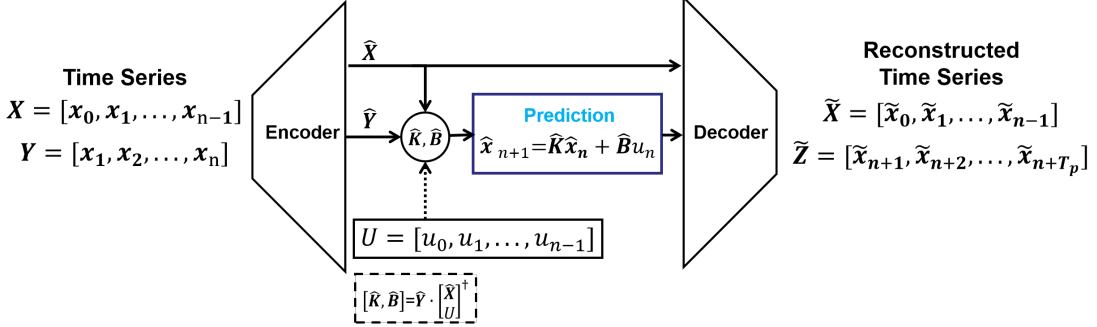


Fig. 3. The deep Koopman operator model. The encoder and decoder are composed of three fully-connected layers. We input the past n steps of time series x_0, x_1, \dots, x_{n-1} and current state x_n (i.e., $X = [x_0, x_1, \dots, x_{n-1}]$ and $Y = [x_1, \dots, x_n]$) into the encoder and transform them into a high-dimensional space, where we calculate/update the Koopman operator \hat{K} and the control matrix \hat{B} (with external input U). A linear dynamical system, $\hat{x}_{n+1} = \hat{K}\hat{x}_n + \hat{B}u_n$, is lying on this high-dimensional space. Given \hat{K} and \hat{B} , the next T_p steps of time series can be predicted. Then, the predicted signals (i.e., $\hat{x}_{n+i}, i = \{1, \dots, T_p\}$) and \hat{X} are converted back to the original space by the decoder. In the deep Koopman operator model, network parameters, the Koopman operator \hat{K} and the control matrix \hat{B} are learned in a self-supervised manner.

B. Definition of Explicit Loss Function

The objective of the deep Koopman operator based autoencoder is to learn a finite invariant subspace that approximates the Koopman operator. The loss is specifically designed with different theoretical considerations for learning the finite-dimensional approximated Koopman operator and building the linear dynamical system. In summary, the explicit loss function for training the deep Koopman operator model covers the following reconstruction term and prediction-reconstruction term with Mean-Squared Error (MSE).

(1) Reconstruction error of X :

$$\mathcal{L}_{\text{recon}} = \frac{1}{n * \text{dim}} \|X - \tilde{X}\|_2^2, \quad (16)$$

(2) Prediction-reconstruction error:

$$\mathcal{L}_{\text{pred}} = \frac{1}{T_p * \text{dim}} \sum_{i=1}^{T_p} \|x_{n+i} - \tilde{x}_{n+i}\|_2^2, \quad (17)$$

where dim is the dimension of the original state space. n is the number of steps in both X and \tilde{X} . T_p is the length of prediction.

The total loss function can be summarized as

$$\mathcal{L} = \lambda_{\text{recon}} \mathcal{L}_{\text{recon}} + \lambda_{\text{pred}} \mathcal{L}_{\text{pred}} \quad (18)$$

where λ_{recon} and λ_{pred} are the hyper-parameters to balance the reconstruction error and prediction-reconstruction error. In our study, we set them equal to 1 by default.

Our proposed deep Koopman operator model aims to learn an invariant linear subspace of seizure dynamics for seizure prediction and the subsequent MPC-based optimization of neurostimulation strategy.

III. EXPERIMENTS AND RESULTS

We first test the performance of the deep Koopman operator model on fitting and predicting epileptic EEG using synthetic data and real data, and then test the performance of Koopman-MPC framework on seizure suppression on a simulation platform.

A. Dataset Description

The deep Koopman operator model is validated with both synthetic data and real data. We used the well-known Jansen-Rit model [41] to generate EEG data. By changing the model parameter (i.e., the excitatory synaptic gain, A), Jansen-Rit model can synthesize the seizure-free EEG and seizure EEG signals. In our study, we mimic seizure propagation process in two distant interconnected cortical columns by a double cortical columns Jansen-Rit model described in Appendix Eq. (21). The seizure propagates from the epileptogenic foci ($A = 7.8$) to a seizure-free region ($A = 7.0$). We synthesize seizure-like waves with 50 Hz sampling rate by inserting random inputs in seizure cortex in Jansen-Rit model. An example of synthetic data is shown in Fig. 4(A). A description of parameters of the Jansen-Rit model is detailed in Appendix (Table VI).

The real data, an open dataset from American Epilepsy Society Seizure Prediction Challenge in Kaggle (<https://www.kaggle.com/c/seizure-prediction>), includes iEEG signals during pre-ictal (an hour) and interictal period (an hour) with 5000Hz sampling rate. Take the interictal iEEG data of the first patient as an example shown in Fig. 4(B). We down sample the original data (5000 Hz) into 500Hz for reducing memory storage and speed up computation during long-period (tens of millisecond level) estimation and prediction.

The synthetic and real data are separated into the corresponding training set (80%) and testing set (20%). In each testing, 200 consecutive time steps are predicted (Fig. 6). 10 steps are predicted each time and 20-time predictions are concatenated. For each time, we first update the approximated Koopman operator using the data from the past $n = 40$ steps and then predict the future $T_p = 10$ steps from the current step as described by the Eq. (12) or Eq. (13).

B. Baseline models and evaluation metrics

The Koopman operator model is compared with a 10-order autoregressive model (the order is the number of preceding data that are used to predict the value at the present time) and a Gated Recurrent Units mode model (GRU, a variant of

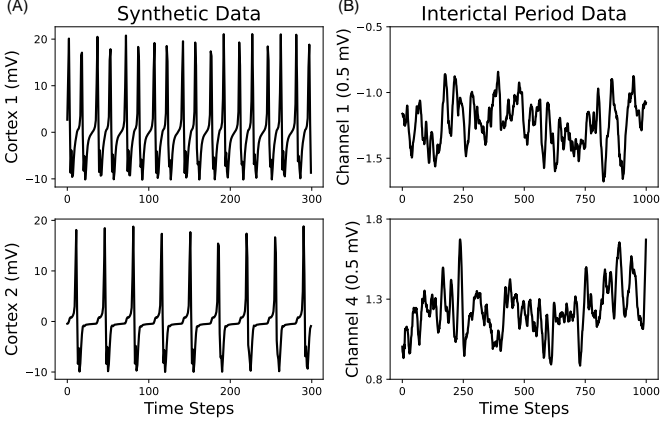


Fig. 4. The visualization of the synthetic data and real data. (A) synthetic seizure-like waves propagating from the epileptogenic foci (up) to a seizure-free cortex (bottom), (B) interictal real data from two iEEG channels.

RNN model), in terms of the accuracy of data prediction. We introduce two quantitative metrics for T_p -step prediction: the Mean-Squared-Error (MSE) and the R-Square (R^2).

$$\text{MSE} = \frac{1}{T_{\text{pred}}} \sum_{k=1}^{T_{\text{pred}}} \|y_k - \hat{y}_k\|_2^2$$

$$R^2 = 1 - \frac{\sum_{k=1}^{T_{\text{pred}}} (y_k - \hat{y}_k)^2}{\sum_{k=1}^{T_{\text{pred}}} (y_k - \bar{y})^2} \quad (19)$$

where \hat{y}_k is the predicted data, y_k is the ground-truth seizure series, and \bar{y} is the average activity of the ground truth (GT). T_{pred} is the temporal length of prediction. Here, MSE and R^2 quantify the averaged error and the similarity between the predicted data and the ground truth, respectively. The lower MSE and the higher R^2 , the better the seizure prediction.

For the seizure control, the RNN-MPC controller is considered as a baseline model. We evaluate the running time of each step of MPC solving process under the same hardware configuration (Intel Core i5-7600K CPU with a frequency of 3.80 GHz and a RAM of 16.00 GB).

C. Prediction of Seizure Dynamics

In the training phase for the Koopman operator model, network parameters (*e.g.*, the encoder and the decoder), the Koopman operator, and the control matrix are learned. After the network parameters are learned, the Koopman operator and the control matrix can be updated in real time. Thus, the main objective in the training is to learn an invariant subspace for estimating Koopman operator \hat{K} . We use the past $n = 40$ steps of seizure signals to estimate the Koopman operator $\hat{K} \in \mathbb{R}^{m \times m}$ ($m = 12$ for synthetic data and $m=16$ for real data) and the control matrix $\hat{B} \in \mathbb{R}^{m \times r}$ ($m = 12, r = 1$ for synthetic data; $m = 16, r = 0$ for real data), and predict the future $T_p = 10$ steps of hidden states as described in Sec. II-A. The prediction in high dimensional space is then transformed back into the original space for calculating prediction-reconstruction error.

In the test phase, we fix the network parameters and recalibrate the Koopman operator based on the $n = 40$ preceding

steps of signals and the prediction of the next $T_p = 10$ steps of signals in the learnt invariant embedding space. To be noted, in the setting of Koopman operator model, $n > m$ guarantees the full-rankness of the inverse term for computing the pseudo inverse matrix in Eq. (5).

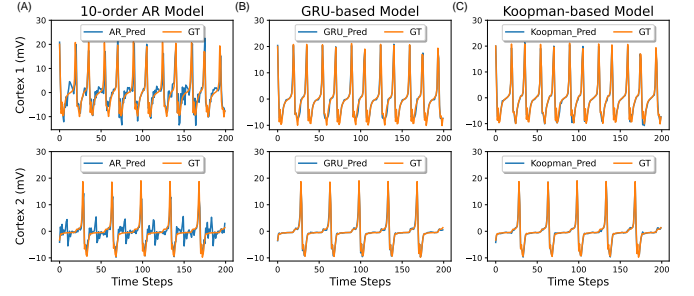


Fig. 5. The prediction of seizure dynamics using synthetic seizure-like EEG waves generated by two cortical columns model: (A) 10-order autoregressive model; (B) GRU-based model; (C) Deep Koopman operator model using koopman-2 (# of param. = 854).

TABLE I
THE PREDICTION PERFORMANCE IN THE SYNTHETIC DATA.

Model	# of param.	MSE	R^2
10-order AR	0	1.0676 \pm 0.4063	0.6829 \pm 0.0314
GRU (Synthetic)	967	0.8970 \pm 0.1433	0.9793 \pm 0.0029
Koopman-1	686	1.3215 \pm 0.3589	0.9652 \pm 0.0109
Koopman-2	854	1.0529 \pm 0.3387	0.9726 \pm 0.0109
Koopman-3	1038	0.7763\pm0.1911	0.9797\pm0.0055

The GRU-based predictive model consists of a *encoder network* (two dense connected layers, and only the first layer followed with tanh activation function) which takes the past 10-step observation signals and 9-step input signals as inputs, a *GRU network* (10 dimensions for synthetic data and 16 dimensions for real data) which recurrently generate the next $T_p = 10$ steps of hidden states, and a *decoder network* (two dense connected layers, and only the first layer followed with tanh activation function) to convert the 10 steps of hidden states back to the original state space. The GRU-based model settings are summarized in Appendix (Table V). To train these three modules in GRU-based network (*i.e.*, the encoder, the GRU, and the decoder), the loss function is formulated as minimizing the prediction error. Notably, both the GRU-based model and Koopman-based model are composed of an encoder, a decoder and a part of dynamical system. The main difference is rooted in the nonlinear system dynamics in the hidden state space characterized by a GRU network, and the linear system dynamics characterized by a Koopman operator in Koopman-based model.

The 10-order AR model is not needed to train an additional model for space transformation. It only updates the parameter of the AR model by the past 40 steps signals and then predicts the future $T_p = 10$ steps signals.

The results from the synthetic data of double cortical columns are shown in Fig. 5 and Table I. Specifically, Fig. 5 illustrates the prediction of temporal evolution when using the Koopman operator based model and baseline models. As we can see, both the deep learning models (*i.e.*, Koopman operator

based model and the GRU model) can predict future dynamics well. The quantification of three metrics (*i.e.*, # of parameters, MSE and R^2) are listed in Table I. To be noted, Koopman 1, 2 and 3 share the same network architecture, and the only difference is the output dimension of hidden layer and final layer, as shown in Appendix (Table IV). Table I demonstrates that the Koopman-3 model outperforms the baseline models. More importantly, the performance from the smaller Koopman-based models (Koopman-1 and Koopman-2) approximate to a GRU-based nonlinear dynamical system. The results suggest that the Koopman operator model can transform the low-dimensional ($k = 2$) nonlinear dynamical system into a finite-dimensional ($m = 12$) linear forward system.

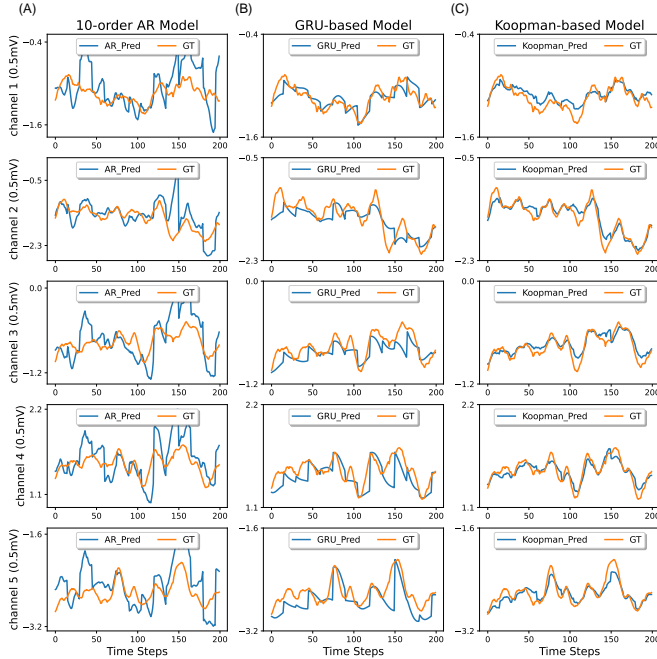


Fig. 6. The visualization of prediction of real interictal signals (5 iEEG channels). (A) 10-order autoregressive model; (B) GRU-based model; (C) Koopman operator model.

TABLE II
THE PREDICTION PERFORMANCE IN THE REAL DATA.

Model	# of param.	MSE	R^2
10-order AR	0	0.2716 ± 0.4611	0.02832 ± 0.1503
GRU (Real)	2.6K	0.0200 ± 0.0107	0.4757 ± 0.1634
Koopman	1813	0.0053 ± 0.0046	0.8910 ± 0.0340

The prediction results from the real iEEG data with 5 channels are shown in Fig. 6 and Table II. Fig. 6 visualizes the prediction of dynamics using Koopman-based model, compared with the 10-order AR model and a GRU-based model. It is obvious that the 10-order AR model cannot capture the system dynamics. Compared with the GRU-based model, the Koopman-based model can better predict the interictal real data. The quantification of three metrics in Table II indicates that the deep Koopman operator based model outperforms the two baseline models in predicting the real epileptic dynamics. In particular, despite the highly complex nonlinearity in the

GRU-based model (# = 2.6K), a simpler Koopman-based linear dynamical model with a much smaller parameter size (# = 1.8K) can provide the lower MSE and higher R^2 .

Together with results from synthetic data and real data, the proposed deep Koopman operator model can learn a finite dimensional invariant subspace to transform the original nonlinear dynamical system to a linear system to predict future states. The dynamics of the entire system is embedded into the approximated Koopman operator \hat{K} and the control matrix \hat{B} which can be re-calibrated at each step, supporting the flexibility of online learning. In contrast, the GRU-based model learns the hidden nonlinear dynamics and evolves under a fixed dynamical law. Its system properties are not updated online. The autoregressive model fails to capture the nonlinear dynamics in the predictions. Therefore, the deep Koopman operator based model is a better predictive model than the two baseline models.

D. MPC-based Seizure Suppression

Since the seizure dynamics are highly nonlinear, it is difficult for a predictive model to track seizure dynamics over long periods of time. To address this issue, the Koopman operator \hat{K} and control matrix \hat{B} in the Koopman-MPC model is periodically re-estimated and re-calibrated. After the linear dynamical system parameters are updated, the optimal neurostimulation strategy ($\Delta u \in \mathbb{R}^{r \times T_c}$, $r=1$ is the input dimension in control the seizure cortex and T_c is the length of control horizon) under MPC framework is solved by using the standard linear quadratic programming solver. To be noted, the network parameters in Koopman-based models and GRU-based models are not updated once the models have been trained. Only the the Koopman operator \hat{K} and control matrix \hat{B} are online updated.

Here we test the performance of the MPC-based framework in seizure suppression. We examine the control ability and computational efficiency of MPC optimization in seizure suppression, using the Koopman-based model and the GRU-based model.

In GRU-MPC framework, the hidden states lie in a highly nonlinear space, rather than the linear space (Eq. (10)) in Koopman-MPC framework. Thus, the nonlinear dynamical system in GRU-based model constructs a highly nonlinear optimization problem in MPC, which cannot be solved simply by a quadratic programming solver. To this end, we use a deep learning solution with the gradient descent for optimization. Specifically, we transfer the GRU-MPC optimization problem into a pyTorch framework and solve it with the Adam solver (with a fixed learning rate of 0.01 and 10-step iterations).

We conducted numerical experiments on Jensen-Rit simulation platform to test the effects of Koopman-MPC framework on seizure control. We set a 10-step predictive horizon and a 10-step control horizon to obtain the optimal control signal for seizure suppression. Fig. 7 shows the suppressed seizure signals (top and middle) and the corresponding control signals (bottom), which are provided by the GRU-MPC controller (Fig. 7A) and Koopman-MPC controller (Fig. 7B). In each experiment, we first collect some input-output data for updating

the model parameters in the deep Koopman operator model, as well as initializing the hidden state of the GRU model. Then, the optimal control signal is designed by MPC controller and inserted into the Jansen Rit model. In Fig. 7, although both models successfully suppress the seizures, the Koopman-MPC controller responds faster. This is further confirmed by the quantification of the computational efficiency in Table III. The Koopman operator MPC model only takes 0.035 second to obtain the optimal control signal, which is sufficiently fast for the closed-loop neurostimulation applications.

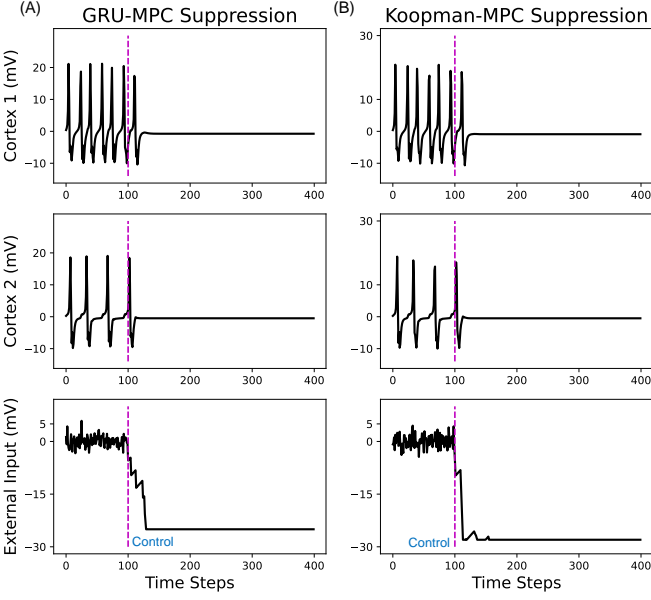


Fig. 7. Effects of MPC-based controller on seizure control. (A) GRU-MPC seizure control; (B) Koopman-MPC seizure control. The experiments are conducted on the simulation platform using Jensen-Rit Model. The results show both controllers start to insert control signal at time step=100 and successfully suppress seizures, but Koopman-MPC controller responds faster.

TABLE III
THE COMPUTATIONAL EFFICIENCY OF NUMERICAL OPTIMIZATION

Model	model properties	Running time (s)
GRU-MPC	10-dim nonlinear model	0.139±0.004
Koopman-MPC	12-dim linear model	0.035±0.009

E. Online Learning of Koopman Operator for closed-loop neurostimulation

We further test whether the online learning Koopman-MPC framework can predict and control seizures during the state transition process (from seizure-free to seizure). Note that the Koopman operator model acts on the invariant subspace which is only trained with seizure data. We simulated the EEG signals transiting from the seizure-free state to the seizure state by varying the excitatory gain parameter A . Specifically, it simulates the non-ictal state $A = 7.0$ for the first 200 steps, shifts to the ictal period $A = 7.8$ for the next 200 steps, and eventually turns to non-ictal state $A = 7.0$ again for the last 200 steps.

The online prediction of the state transitions is shown in Fig. 8(A-B). Attribute to the online learning nature of the

Koopman operator, the Koopman-based model can track the system dynamics better than the GRU-based model, during both the seizure-free period and seizure period. The results confirm that the learned invariant subspace is generalizable to the seizure-free and postictal states. The online updates of Koopman operator \hat{K} provide flexibility to track the transition states.

To investigate the system stability and spectral information of the neural system during epileptic period, we conduct eigendecomposition on the estimated Koopman operator \hat{K} as Eq. (3). Fig. 8(C) shows the estimated maximum complex part of the eigenvalues of \hat{K} in spectral analysis, reflecting the maximum frequency of the seizure dynamics. Our results demonstrate the maximum spectral of the system is largely increased at seizure onset, well in line with Li et al [42]. The results suggest that our Koopman-based model has great potential to offer a biomarker of seizure onset.

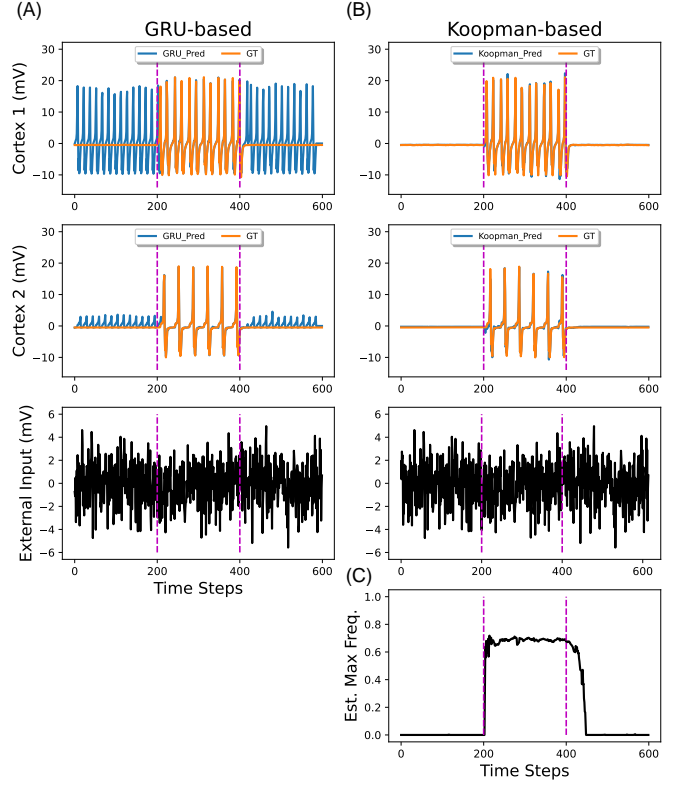


Fig. 8. Online learning to predict seizure dynamics with the state transition from preictal, to ictal and finally postictal states. (A) GRU-based prediction; (B) Koopman operator based prediction; (C) The estimated maximal complex part of eigenvalues of the approximated Koopman operator \hat{K} . From top to bottom, we display the neural signals in cortex 1 (the epileptic foci), in cortex 2 (the transmission area) and the control signals.

Inspired by the results of spectral analysis, we design a closed-loop neurostimulation system based on the Koopman-MPC framework, using the maximum frequency of the estimated Koopman operator \hat{K} as a biomarker. According to Fig. 8(C), we set a threshold $f_{\text{threshold}} = 0.1$ for the maximum frequency. Once the maximum frequency of \hat{K} is larger than the threshold ($f > f_{\text{threshold}}$), the controller is actuated and triggers the neurostimulation to suppress seizure-like waves. We conduct experiments to validate our closed-loop neu-

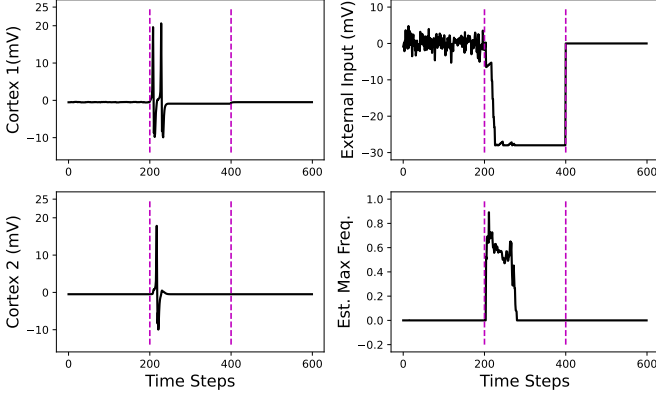


Fig. 9. Online learning for closed-loop neuromodulation using Koopman-MPC framework. The Koopman operator \hat{K} is updated step by step, and we set a threshold on the maximal frequency (*i.e.*, the complex part of eigenvalue) to detect the seizure onset. Once the maximum frequency of \hat{K} is larger than the threshold ($f_{\text{threshold}} = 0.1$), the controller is actuated and triggers the neurostimulation to suppress seizure-like waves. Note, in the first 200 steps nonseizure period, we insert random inputs for collecting input-output data.

rostimulation system. As shown in Fig. 9, the neurostimulation is triggered at the 200th step and the seizures are immediately suppressed after the controller being actuated. These results show that Koopman-MPC framework empowers the closed-loop neurostimulation.

IV. DISCUSSION

In this work, we propose a novel deep Koopman-MPC framework for closed-loop electrical neurostimulation. A tailored autoencoder is employed to learn the invariant subspace of the Koopman operator, in which a coordinate transformation maps the nonlinear dynamics into finite-dimensional linear dynamics. The approximation of the Koopman operator provides a sufficient prediction horizon in seizure prediction, which can be integrated into the MPC controller for seizure suppression.

A. Prediction and Control for Seizure Dynamics

The epileptic seizures can be modelled as a dynamical system [20], [21], [22]. System identification is essential for modeling and prediction of seizure dynamics, contributing to optimizing neurostimulation strategies in model-based seizure suppression [21]. Considering the controlability and interpretability, the accuracy and the complexity of the model need to be balanced when identifying the system dynamics, especially when the model is combined with a MPC controller for designing optimal neurostimulation in real-time. The proposed Koopman operator based model has higher prediction accuracy compared with a 10-order AR model and a GRU-based model (Table I and II), while maintaining a considerable size of network parameters. One possible reason is that the Koopman model learns an invariant subspace which captures sufficient nonlinear patterns in the approximated Koopman operator for seizure prediction [43]. A great merit of the Koopman-based model is its ability to online update the Koopman operator, whereas the GRU-based model cannot update its governing function. Another merit of the Koopman model is its linear

property, which greatly facilitates the convex optimization in MPC control and provides a unique optimal solution with high computational efficiency (Table III). In contrast, the GRU-based MPC model is a highly nonlinear optimization problem which is numerical computational inefficiency. In fact, it is most likely a trade-off between model complexity and computational efficiency when designing models for real-time control. A higher-order complex model might better identify the system, but it is computationally expensive in optimization. Importantly, the proposed Koopman-MPC framework, to some extent, breaks the speed-accuracy tradeoff by combining a finite-dimensional approximated Koopman operator model and a linear MPC optimal controller.

B. Seizure simulation platform

For ethical reasons, it is difficult to directly collect input-output data of patients with epilepsy. Therefore, using a computational model to generate neural dynamics is an alternative way for the verification of control strategies [44], [45]. In this study, we applied the Jansen-Rit model to validate the Koopman model for seizure prediction and to test the neurostimulation policy produced by MPC controller. As a macroscopic cortical column-level neural mass model, the Jansen-Rit model accounts for three populations of cells dynamical interactions (*i.e.*, excitatory, inhibitory, and pyramidal neuron populations) [41]. By varying the parameters, the model can generate neural activity in healthy or seizure conditions. For instance, the bifurcation parameters control the critical point which reflects the transitions between stable and unstable states. The average excitatory synaptic gain parameter manipulates the dynamic pattern of healthy EEG and epilepsy [41]. Also, many other dynamical models have been proposed to simulate neurodynamics with physics laws in health or epilepsy from the microscopic level [23] to the macroscopic level [22], [46], [47], [48]. Kuramoto model, as a phase oscillator, is used to synthesize the fMRI phase dynamics series [47], and even used to study the cognitive process [49], [50]. A focal epileptic network dynamical model based on scale-free network connectivity is used to simulate spontaneous epilepsy dynamics [48]. It would be of high interest to build a more realistic seizure simulation platform for testing different control policies and even for performing virtual surgery.

C. Limitations and future works

It is worthy to mention some limitations and possible future directions of our work. First, we did not collect input-output data from epilepsy patients in a biological experiment. Instead, we ran numerical experiments with Jansen-Rit model to simulate the EEG data and conduct MPC control. Second, our proposed Koopman operator based model cannot perform as a stochastic model to estimate the probability of seizure occurrence. Integrating a probabilistic model for seizure prediction and classification [25], [51] into our framework is our future work to further improve neurostimulation performance [15]. Third, we did not examine the the controllability of the identified system, which can be characterized

by the approximated Koopman operator and control matrix. The controllability properties of the linear dynamical system will enable the system to reach any state in finite control steps [52]. A controllable approximated Koopman operator based model will broadly advance neuroscience applications (e.g., cognitive control, neurofeedback control). Fourth, we did not consider the measurement noise in model fitting. The EEG denoising techniques [53], [54] will contribute to the robustness of Koopman-based models in real applications. Also, the eigendecomposition of the approximated Koopman operator reflects the spectral information about the system dynamics [38]. A comprehensive study on the spectral properties of the Koopman operator learned from EEG and epilepsy dynamics is one of our future work.

The brain is a complex coupled dynamical system [55], [56]. Modelling and controlling the brain network while balancing the speed and accuracy is challenging. The development of neuromodulation techniques and cybernetics will promote each other. In our work, we only consider two cortical regions dynamics and its neuromodulation, controlling the complex brain network dynamics calls for hierarchical network models and more advanced control theory [57]. The development of cybernetics would provide new tools for neurostimulation, including the selection of the optimal targeted stimulation regions, the robustness and safety of stimulation protocols [58].

ACKNOWLEDGMENT

The authors gratefully acknowledge Mr. Rongwei Liang for the insightful discussions and editing, Dr. Yi Yao and Prof. Haiyan Wu for the useful discussions.

Authors declare to have no conflict of interests.

REFERENCES

- [1] R. S. Fisher, C. Acevedo, A. Arzimanoglou, A. Bogacz, J. H. Cross, C. E. Elger, J. Engel Jr, L. Forsgren, J. A. French, M. Glynn *et al.*, “Ilae official report: a practical clinical definition of epilepsy,” *Epilepsia*, vol. 55, no. 4, pp. 475–482, 2014.
- [2] J. Yuan, X. Ran, K. Liu, C. Yao, Y. Yao, H. Wu, and Q. Liu, “Machine learning applications on neuroimaging for diagnosis and prognosis of epilepsy: A review,” *Journal of neuroscience methods*, p. 109441, 2021.
- [3] N. M. Wetjen, W. R. Marsh, F. B. Meyer, G. D. Cascino, E. So, J. W. Britton, S. M. Stead, and G. A. Worrell, “Intracranial electroencephalography seizure onset patterns and surgical outcomes in nonlesional extratemporal epilepsy,” *Journal of neurosurgery*, vol. 110, no. 6, pp. 1147–1152, 2009.
- [4] P. Jayakar, J. Gotman, A. S. Harvey, A. Palmini, L. Tassi, D. Schomer, F. Dubeau, F. Bartolomei, A. Yu, P. Krsek *et al.*, “Diagnostic utility of invasive eeg for epilepsy surgery: indications, modalities, and techniques,” *Epilepsia*, vol. 57, no. 11, pp. 1735–1747, 2016.
- [5] D. Cogan, J. Birjandtalab, M. Nourani, J. Harvey, and V. Nagarad, “Multi-biosignal analysis for epileptic seizure monitoring,” *International journal of neural systems*, vol. 27, no. 01, p. 1650031, 2017.
- [6] A. J. Lowe, E. David, C. J. Kilpatrick, Z. Matkovic, M. J. Cook, A. Kaye, and T. J. O’Brien, “Epilepsy surgery for pathologically proven hippocampal sclerosis provides long-term seizure control and improved quality of life,” *Epilepsia*, vol. 45, no. 3, pp. 237–242, 2004.
- [7] S. L. Moshé, E. Perucca, P. Ryvlin, and T. Tomson, “Epilepsy: new advances,” *The Lancet*, vol. 385, no. 9971, pp. 884–898, 2015.
- [8] A. Berényi, M. Belluscio, D. Mao, and G. Buzsáki, “Closed-loop control of epilepsy by transcranial electrical stimulation,” *Science*, vol. 337, no. 6095, pp. 735–737, 2012.
- [9] M. T. Salam, J. L. P. Velazquez, and R. Genov, “Seizure suppression efficacy of closed-loop versus open-loop deep brain stimulation in a rodent model of epilepsy,” *IEEE Transactions on Neural Systems and Rehabilitation Engineering*, vol. 24, no. 6, pp. 710–719, 2015.
- [10] V. Salanova, “Deep brain stimulation for epilepsy,” *Epilepsy & Behavior*, vol. 88, pp. 21–24, 2018.
- [11] M. C. Li and M. J. Cook, “Deep brain stimulation for drug-resistant epilepsy,” *Epilepsia*, vol. 59, no. 2, pp. 273–290, 2018.
- [12] C. C. Oderiz, N. von Ellenrieder, F. Dubeau, A. Eisenberg, J. Gotman, J. Hall, A.-S. Hincapié, D. Hoffmann, A.-S. Job, H. M. Khoo *et al.*, “Association of cortical stimulation-induced seizure with surgical outcome in patients with focal drug-resistant epilepsy,” *JAMA neurology*, vol. 76, no. 9, pp. 1070–1078, 2019.
- [13] R. S. Fisher and A. L. Velasco, “Electrical brain stimulation for epilepsy,” *Nature Reviews Neurology*, vol. 10, no. 5, pp. 261–270, 2014.
- [14] Y. Zheng, Z. Jiang, A. Ping, F. Zhang, J. Zhu, Y. Wang, W. Zhu, and K. Xu, “Acute seizure control efficacy of multi-site closed-loop stimulation in a temporal lobe seizure model,” *IEEE Transactions on Neural Systems and Rehabilitation Engineering*, vol. 27, no. 3, pp. 419–428, 2019.
- [15] K. W. Scangos, A. N. Khambhati, P. M. Daly, G. S. Makhoul, L. P. Sugrue, H. Zamanian, T. X. Liu, V. R. Rao, K. K. Sellers, H. E. Dawes *et al.*, “Closed-loop neuromodulation in an individual with treatment-resistant depression,” *Nature Medicine*, pp. 1–5, 2021.
- [16] C. Liu, C. Zhou, J. Wang, C. Fietkiewicz, and K. A. Loparo, “Delayed feedback-based suppression of pathological oscillations in a neural mass model,” *IEEE Transactions on Cybernetics*, vol. 51, no. 10, pp. 5046–5056, 2019.
- [17] H. Yu, Z. Meng, H. Li, C. Liu, and J. Wang, “Intensity-varied closed-loop noise stimulation for oscillation suppression in the parkinsonian state,” *IEEE Transactions on Cybernetics*, 2021.
- [18] S. Pequito, A. Ashourvan, D. Bassett, B. Litt, and G. J. Pappas, “Spectral control of cortical activity,” in *2017 American Control Conference (ACC)*, 2017.
- [19] A. Ashourvan, S. D. G. M. Pequito, A. N. Khambhati, F. Mikhail, and D. Bassett, “Model-based design for seizure control by stimulation,” *Journal of Neural Engineering*, vol. 17, no. 2, 2020.
- [20] S. Chang, X. Wei, F. Su, C. Liu, G. Yi, J. Wang, C. Han, and Y. Che, “Model predictive control for seizure suppression based on nonlinear auto-regressive moving-average volterra model,” *IEEE Transactions on Neural Systems and Rehabilitation Engineering*, vol. 28, no. 10, pp. 2173–2183, 2020.
- [21] S. Chatterjee, O. Romero, A. Ashourvan, and S. Pequito, “Fractional-order model predictive control as a framework for electrical neurostimulation in epilepsy,” *Journal of Neural Engineering*, vol. 17, no. 6, p. 066017, 2020.
- [22] V. K. Jirsa, W. C. Stacey, P. P. Quilichini, A. I. Ivanov, and C. Bernard, “On the nature of seizure dynamics,” *Brain*, vol. 137, no. 8, pp. 2210–2230, 2014.
- [23] C. D. Verdugo, S. Myren-Svelstad, E. Aydin, E. Van Hoeymissen, C. Deneubourg, S. Vanderhaeghe, J. Vancraeynest, R. Pelgrims, M. I. Cosacak, A. Muto *et al.*, “Glia-neuron interactions underlie state transitions to generalized seizures,” *Nature communications*, vol. 10, no. 1, pp. 1–13, 2019.
- [24] M. Arrais, J. Modolo, D. Mogul, and F. Wendling, “Design of optimal multi-site brain stimulation protocols via neuro-inspired epilepsy models for abatement of interictal discharges,” *Journal of Neural Engineering*, vol. 18, no. 1, p. 016024, 2021.
- [25] Y. Li, Y. Liu, Y.-Z. Guo, X.-F. Liao, B. Hu, and T. Yu, “Spatio-temporal-spectral hierarchical graph convolutional network with semisupervised active learning for patient-specific seizure prediction,” *IEEE Transactions on Cybernetics*, 2021.
- [26] Y. Zhang, Y. Guo, P. Yang, W. Chen, and B. Lo, “Epilepsy seizure prediction on eeg using common spatial pattern and convolutional neural network,” *IEEE Journal of Biomedical and Health Informatics*, vol. 24, no. 2, pp. 465–474, 2019.
- [27] T. Liu, N. D. Truong, A. Nikpour, L. Zhou, and O. Kavehei, “Epileptic seizure classification with symmetric and hybrid bilinear models,” *IEEE journal of biomedical and health informatics*, vol. 24, no. 10, pp. 2844–2851, 2020.
- [28] Y. Yuan, G. Xun, K. Jia, and A. Zhang, “A multi-view deep learning framework for eeg seizure detection,” *IEEE journal of biomedical and health informatics*, vol. 23, no. 1, pp. 83–94, 2018.
- [29] E. Hazan, K. Singh, and C. Zhang, “Learning linear dynamical systems via spectral filtering,” *Advances in Neural Information Processing Systems*, vol. 30, pp. 6702–6712, 2017.
- [30] A. Chiuso and G. Pillonetto, “System identification: A machine learning perspective,” *Annual Review of Control, Robotics, and Autonomous Systems*, vol. 2, pp. 281–304, 2019.

[31] N. Lanzetti, Y. Z. Lian, A. Cortinovis, L. Dominguez, M. Mercangöz, and C. Jones, "Recurrent neural network based mpc for process industries," in *2019 18th European Control Conference (ECC)*. IEEE, 2019, pp. 1005–1010.

[32] A. Wikner, J. Pathak, B. Hunt, M. Girvan, T. Arcomano, I. Szunyogh, A. Pomerance, and E. Ott, "Combining machine learning with knowledge-based modeling for scalable forecasting and subgrid-scale closure of large, complex, spatiotemporal systems," *Chaos: An Interdisciplinary Journal of Nonlinear Science*, vol. 30, no. 5, p. 053111, 2020.

[33] K. Bieker, S. Peitz, S. L. Brunton, J. N. Kutz, and M. Dellnitz, "Deep model predictive flow control with limited sensor data and online learning," *Theoretical and Computational Fluid Dynamics*, pp. 1–15, 2020.

[34] Andrzej, *Chaos, fractals, and noise : stochastic aspects of dynamics /2nd ed.* Springer-Verlag, 1994.

[35] B. O. Koopman, "Hamiltonian systems and transformation in hilbert space," *Proceedings of the national academy of sciences of the united states of america*, vol. 17, no. 5, p. 315, 1931.

[36] N. Takeishi, Y. Kawahara, and T. Yairi, "Learning koopman invariant subspaces for dynamic mode decomposition," in *Proceedings of the 31st International Conference on Neural Information Processing Systems*, 2017, pp. 1130–1140.

[37] J. Morton, F. D. Witherden, A. Jameson, and M. J. Kochenderfer, "Deep dynamical modeling and control of unsteady fluid flows," in *Proceedings of the 32nd International Conference on Neural Information Processing Systems*, 2018, pp. 9278–9288.

[38] M. Korda, M. Putinar, and I. Mezić, "Data-driven spectral analysis of the koopman operator," *Applied and Computational Harmonic Analysis*, vol. 48, no. 2, pp. 599–629, 2020.

[39] M. O. Williams, I. G. Kevrekidis, and C. W. Rowley, "A data-driven approximation of the koopman operator: Extending dynamic mode decomposition," *Journal of Nonlinear Science*, vol. 25, no. 6, pp. 1307–1346, 2015.

[40] E. Yeung, S. Kundu, and N. Hodas, "Learning deep neural network representations for koopman operators of nonlinear dynamical systems," in *2019 American Control Conference (ACC)*. IEEE, 2019, pp. 4832–4839.

[41] B. H. Jansen and V. G. Rit, "Electroencephalogram and visual evoked potential generation in a mathematical model of coupled cortical columns," *Biological cybernetics*, vol. 73, no. 4, pp. 357–366, 1995.

[42] A. Li, C. Huynh, Z. Fitzgerald, I. Cajigas, D. Brusko, J. Jagid, A. O. Claudio, A. M. Kanner, J. Hopp, S. Chen *et al.*, "Neural fragility as an eeg marker of the seizure onset zone," *Nature neuroscience*, vol. 24, no. 10, pp. 1465–1474, 2021.

[43] B. Lusch, J. N. Kutz, and S. L. Brunton, "Deep learning for universal linear embeddings of nonlinear dynamics," *Nature communications*, vol. 9, no. 1, pp. 1–10, 2018.

[44] T. Kajishima and K. Taira, "Computational fluid dynamics," *Cham: Springer International Publishing*, no. 1, 2017.

[45] A. L. Hodgkin and A. F. Huxley, "A quantitative description of membrane current and its application to conduction and excitation in nerve," *The Journal of physiology*, vol. 117, no. 4, pp. 500–544, 1952.

[46] D. Fan and Q. Wang, "Closed-loop control of absence seizures inspired by feedback modulation of basal ganglia to the corticothalamic circuit," *IEEE Transactions on Neural Systems and Rehabilitation Engineering*, vol. 28, no. 3, pp. 581–590, 2020.

[47] M. Fukushima and O. Sporns, "Structural determinants of dynamic fluctuations between segregation and integration on the human connectome," *Communications biology*, vol. 3, no. 1, pp. 1–11, 2020.

[48] L. Zhang, Q. Wang, and G. Baier, "Dynamical features of a focal epileptogenic network model for stimulation-based control," *IEEE Transactions on Neural Systems and Rehabilitation Engineering*, vol. 28, no. 8, pp. 1856–1865, 2020.

[49] S. Zheng, Z. Liang, Y. Qu, Q. Wu, H. Wu, and Q. Liu, "Kuramoto model-based analysis reveals oxytocin effects on brain network dynamics," *International journal of neural systems*, vol. 32, no. 2, 2022.

[50] C. Bick, M. Goodfellow, C. R. Laing, and E. A. Martens, "Understanding the dynamics of biological and neural oscillator networks through exact mean-field reductions: a review," *The Journal of Mathematical Neuroscience*, vol. 10, pp. 1–43, 2020.

[51] A. Burrello, S. Benatti, K. Schindler, L. Benini, and A. Rahimi, "An ensemble of hyperdimensional classifiers: hardware-friendly short-latency seizure detection with automatic ieeg electrode selection," *IEEE journal of biomedical and health informatics*, vol. 25, no. 4, pp. 935–946, 2020.

[52] Y. Han, W. Hao, and U. Vaidya, "Deep learning of koopman representation for control," in *2020 59th IEEE Conference on Decision and Control (CDC)*. IEEE, 2020, pp. 1890–1895.

[53] H. Zhang, M. Zhao, C. Wei, D. Mantini, Z. Li, and Q. Liu, "Eeg-denoisenet: A benchmark dataset for deep learning solutions of eeg denoising," *Journal of Neural Engineering*, vol. 18, no. 5, p. 056057, 2021.

[54] J. Yu, C. Li, K. Lou, C. Wei, and Q. Liu, "Embedding decomposition for artifacts removal in eeg signals," *arXiv preprint arXiv:2112.00989*, 2021.

[55] E. Bullmore and O. Sporns, "The economy of brain network organization," *Nature reviews neuroscience*, vol. 13, no. 5, pp. 336–349, 2012.

[56] Q. Liu, S. Farahibozorg, C. Porcaro, N. Wenderoth, and D. Mantini, "Detecting large-scale networks in the human brain using high-density electroencephalography," *Human brain mapping*, vol. 38, no. 9, pp. 4631–4643, 2017.

[57] Y. Nakahira, Q. Liu, T. J. Sejnowski, and J. C. Doyle, "Diversity-enabled sweet spots in layered architectures and speed–accuracy trade-offs in sensorimotor control," *Proceedings of the National Academy of Sciences*, vol. 118, no. 22, 2021.

[58] Y. Yuan, X. Tang, W. Zhou, W. Pan, X. Li, H.-T. Zhang, H. Ding, and J. Goncalves, "Data driven discovery of cyber physical systems," *Nature communications*, vol. 10, no. 1, pp. 1–9, 2019.

APPENDIX

A. Model Architecture and its Parameter Setting

The proposed deep Koopman operator model includes encoder and decoder which contain three dense connected layers, except the last layer, other dense connected layers are followed by hyperbolic tangent activation function (Tanh). We summarized the output dimension of each layer as shown in Table IV.

TABLE IV
THE OUTPUT DIMENSION OF EACH LAYER.

Model	module	1st layer	2nd layer	3rd layer
Koopman-1	Encoder	12	12	12
	Decoder	12	12	2
Koopman-2	Encoder	14	14	12
	Decoder	14	14	2
Koopman-3	Encoder	16	16	12
	Decoder	16	16	2
Koopman (real data)	Encoder	16	16	16
	Decoder	16	16	5

The baseline GRU-based model is equipped with three modules, the Initialized module, GRU-module and Output module, we summarized then as Table V.

TABLE V
THE ARCHITECTURE OF EACH MODULE.

Module	Architecture (synthetic data)	Architecture (real data)
Initialized	dense (out dim:5)	dense (out dim:8)
	Tanh()	Tanh()
	dense (out dim:10)	dense (out dim:16)
GRU-module	GRU (in dim:1 out dim:10)	GRU (in dim:0 out dim:16)
	dense (out dim:5)	dense (out dim:8)
	Tanh()	Tanh()
Output	dense (out dim:2)	dense (out dim:5)
	Tanh()	

B. Jansen-Rit Model

The Jansen-Rit model was originally proposed by Jansen and Rit in 1995 for studying the cortical column [41]. It is a neural population model of a local cortical circuit.

In particular, the neural dynamical model consists of three subpopulations, the pyramidal cells, the excitatory feedback interneurons and the inhibitory feedback interneurons, which summarized the following dynamical model.

$$\begin{cases} \dot{y}_1 = y_4 \\ \dot{y}_4 = AaS(y_2 - y_3) - 2ay_4 - a^2y_1 \\ \dot{y}_2 = y_5 + d(t) \\ \dot{y}_5 = Aa(p + C_2S(C_1y_1)) - 2ay_5 - a^2y_2 \\ \dot{y}_3 = y_6 \\ \dot{y}_6 = BbC_4S(C_3y_1) - 2by_6 - b^2y_3 \end{cases} \quad (20)$$

where the Sigmoid function is $S(v) = \frac{2e_0}{1+e^{r(v_0-v)}}$. The model can be extended into double interconnected cortical Jansen-Rit model as,

$$\begin{cases} \dot{y}_0 = y_3 \\ \dot{y}_3 = AaS(y_1 - y_2) - 2ay_3 - a^2y_0 \\ \dot{y}_1 = y_4 \\ \dot{y}_4 = Aa(p + C_2S(C_1y_0) + K_2y_{13}) - 2ay_4 - a^2y_1 \\ \dot{y}_2 = y_5 \\ \dot{y}_5 = BbC_4S(C_3y_0) - 2by_5 - b^2y_2 \\ \dot{y}_6 = y_9 \\ \dot{y}_9 = A'aS(y_7 - y_8) - 2ay_9 - a^2y_6 \\ \dot{y}_7 = y_{10} \\ \dot{y}_{10} = A'a(p' + C'_2S(C'_1y_6) + K_1y_{12}) - 2ay_{10} - a^2y_7 \\ \dot{y}_8 = y_{11} \\ \dot{y}_{11} = B'bC'_4S(C'_3y_6) - 2by_{11} - b^2y_8(t) \\ \dot{y}_{12} = y_{14} \\ \dot{y}_{14} = A'a_dS(y_1 - y_2) - 2a_dy_{14} - a^2y_{12} \\ \dot{y}_{13} = y_{15} \\ \dot{y}_{15} = A'a_dS(y_7 - y_8) - 2a_dy_{15} - a^2y_{13} \end{cases} \quad (21)$$

Here, we only summarized the parameter of double cortical column Jansen-Rit Model as Table VI.

TABLE VI
PARAMETERS FOR DOUBLE CORTICAL COLUMNS JANSEN-RIT MODEL

Parameters	Description	Values
A	Average excitatory synaptic gain	7.8 mV
B	Average inhibitory synaptic gain	22 mV
C_1	Average synaptic connectivity	135
C_2	Average synaptic connectivity	108
C_3	Average synaptic connectivity	33.75
C_4	Average synaptic connectivity	33.75
A'	Average excitatory synaptic gain	7 mV
B'	Average inhibitory synaptic gain	22 mV
C'_1	Average synaptic connectivity	135
C'_2	Average synaptic connectivity	108
C'_3	Average synaptic connectivity	33.75
C'_4	Average synaptic connectivity	33.75
a_d	Reciprocal of excitatory time constant with latency	$a/3$
a	Reciprocal of excitatory time constant	100 Hz
b	Reciprocal of inhibitory time constant	50 Hz
v_0	Potential at half of the maximum firing rate of Sigmoid function	6 mV
r	Steepness of Sigmoid function	0.56 m/V
e_0	Half of the maximum firing rate of Sigmoid function	2.5 Hz
K_1	Connectivity constants	100
K_2	Connectivity constants	100